THE JOURNAL OF BIOLOGICAL CHEMISTRY
Vol. 275, No. 27, Issue of July 7, pp. 20660–20666, 2000

Printed in U.S.A.

Structural Rearrangements of HIV-1 Tat-responsive RNA upon Binding of Neomycin B*

Received for publication, February 4, 2000, and in revised form, March 15, 2000
Published, JBC Papers in Press, March 27, 2000, DOI 10.1074/jbc.M000920200

Cornelius Faber, Heinrich Sticht, Kristian Schweimer, and Paul Rösch‡

From the Lehrstuhl für Biopolymere, Universität Bayreuth, D-95447 Bayreuth, Germany

Binding of human immunodeficiency virus type 1 (HIV-1) transactivator (Tat) protein to Tat-responsive RNA (TAR) is essential for viral replication and is considered a promising starting point for the design of anti-HIV drugs. NMR spectroscopy indicated that the aminoglycosides neomycin B and ribostamycin bind to TAR and that neomycin is able to inhibit Tat binding to TAR. The solution structure of the neomycin-bound TAR has been determined by NMR spectroscopy. Chemical shift mapping and intermolecular nuclear Overhauser effects define the binding region of the aminoglycosides on TAR and give strong evidence for minor groove binding. Based on 15 nuclear Overhauser effect-derived intermolecular distance restraints, a model structure of the TAR-neomycin complex was calculated. Neomycin is bound in a binding pocket formed by the minor groove of the lower stem and the uridine-rich bulge of TAR, which adopts a conformation different from those known. The neamine core of the aminoglycoside (rings I and II) is covered with the bulge, explaining the inhibition of Tat by an allosteric mechanism. Neomycin reduces the volume of the major groove in which Tat is bound and thus impedes essential protein-RNA contacts.

Antibiotics are chemicals that are active against microorganisms, exerting their function in different ways at various cellular locations. Aminoglycoside antibiotics, for example, target the 30 S subunit of ribosomal RNA and cause mistranslation. Molecules of the neomycin family of aminoglycosides (Fig. 1*a*) bind directly to the A site of 16 S ribosomal RNA (1) and efficiently disturb protein biosynthesis of prokaryotes. Structural studies on the interaction of aminoglycosides with RNAs provided insights into the mechanisms of miscoding (2–4). The antibiotic distorts the structure of the RNA and thus leads to errors in protein biosynthesis. Variations in eukaryotic ribosomal RNA prevent high affinity binding of aminoglycosides to the ribosomes of higher organisms, making them less prone to antibiotic influence and thus rendering the antibiotics valuable medical drugs. Due to the growing problem of antibiotic resistance, caused by only a small number of mutations in the microorganisms, the determinants for antibiotic binding to RNA are of major interest in structural biology. Only a few structures of antibiotic-RNA complexes have been determined experimentally to date, among them the structure of paromomycin in complex with a model oligonucleotide comprising the A site of 16 S rRNA (2) and a low resolution and two high resolution structures of complexes between RNA aptamers and tobramycin or neomycin (5–7).

Aminoglycosides have also been found to bind to group I introns (8), to hammerhead RNA (9), and to human hepatitis δ virus ribozymes (10). These antibiotics also bind to the Rev (regulator of expression of the virion) and Tat (transactivator of transcription) binding regions of human immunodeficiency virus type 1 (HIV-1)[1] RNA, Rev response element (11), and Tat-responsive element (TAR) (12). Different modeling approaches yielded several structural models of complexes between neomycin and group I intron (13), hammerhead ribozyme (14), and Rev response element (15). In all of these complexes, the aminoglycoside is bound in the major groove of the RNA duplex at positions where the regular A-helical geometry is distorted by internal loops, bulged out nucleotides, or nonregular base pairs. No additional common structural features of the RNAs are evident. In contrast, the three aminoglycoside-RNA aptamer complexes show a bulged out nucleotide that flaps over the antibiotic forming a binding cavity, whereas the major groove of the A site RNA, favored by an internal loop, is simply widened upon paromomycin binding (2, 3).

Studies of the HIV-1 TAR RNA-neomycin interaction revealed that TAR also undergoes a conformational change upon antibiotic binding (16). TAR forms a base-paired stem closed by an apical loop (Fig. 1*b*). A triple-U bulge interrupts the stem only four base pairs below the loop and divides it into a lower and an upper part. The binding region of neomycin has been identified in the bulge and lower stem region, and competition experiments have shown that neomycin inhibits the HIV-1 Tat binding to TAR (16). Tat is an essential transcription factor for viral replication that binds to the human cellular protein cyclin T1 and to the stem-loop structure of TAR (17). The ternary complex of human cyclin T1, interacting with the loop, and Tat, interacting with the major groove in the bulge region of TAR, causes cyclin-dependent kinase 9 to hyperphosphorylate the COOH-terminal domain of RNA polymerase II, allowing efficient transcription of the viral genome. Inhibition of Tat binding to TAR represses recruitment of cyclin-dependent kinase 9, thus inhibiting phosphorylation of RNA polymerase II and rendering transcription nonprocessive. Thus, the Tat-TAR-human cyclin T1 interaction is an ideal target for drugs against HIV. Understanding of the binary interaction between Tat and

* The costs of publication of this article were defrayed in part by the payment of page charges. This article must therefore be hereby marked "*advertisement*" in accordance with 18 U.S.C. Section 1734 solely to indicate this fact.

The atomic coordinates and structure factors (code 1qd3) have been deposited in the Protein Data Bank, Research Collaboratory for Structural Bioinformatics, Rutgers University, New Brunswick, NJ (http://www.rcsb.org/).

‡ Supported by the Sonderforschungsbereich 466 and the Fonds der Chemischen Industrie. To whom correspondence should be addressed. Tel.: 49-921-55-35-40; Fax: 49-921-55-35-44; paul.roesch@uni-bayreuth.de.

[1] The abbreviations used are: HIV, human immunodeficiency virus; MD, molecular dynamics; TAR, Tat-responsive element; NOE, nuclear Overhauser effect; NOESY, NOE spectroscopy; TOCSY, total correlation spectroscopy; r.m.s., root mean square.

TAR and their inhibition may serve as an initial step for studying the much more complicated ternary complex.

MATERIALS AND METHODS

Neomycin B sulfate was from Roth (Karlsruhe, Germany), ribostamycin sulfate was from ICN (Aurora), and BP3 was chemically synthesized (German Cancer Research Institute, Heidelberg).

RNA Synthesis and Sample Preparation—HIV-1 TAR RNA was synthesized by *in vitro* transcription using T7 polymerase and a synthetic DNA template (CGGTCTAAACTCGGTCCCACGAGAGACCG; MWG Biotech, Ebersberg, Germany). For preparation of selectively $^{13}C/^{15}N$-labeled TAR, uniformly labeled adenosine, cytidine, and uridine triphosphates (Campro Scientific, Emmerich) were used.

To achieve the desired hairpin fold, the TAR was heated to above 80 °C for at least 5 min in 100 mM NaCl, 50 mM potassium phosphate, pH 6.4, and then cooled to room temperature on ice. The correct fold was monitored by NMR spectroscopy. Folded TAR was desalted by dialysis and then freeze-dried. The freeze-dried TAR was resuspended in NMR buffer containing 90 mM NaCl, 18 mM potassium phosphate, pH 6.4, in H_2O/D_2O (9:1, v/v), or D_2O only. Aminoglycosides were added to the RNA from a stock solution (50 mM in NMR buffer).

NMR Spectroscopy—All NMR experiments were performed at 28 and 35 °C on Bruker DRX600 and DMX750 spectrometers at 600 and 750 MHz, respectively, with *xyz*-gradient units. RNA concentrations of the samples used for one-dimensional NMR spectroscopy were 0.2 mM; RNA concentrations for two- and three-dimensional experiments were 2.0 mM for free TAR, 5.0 mM for unlabeled TAR with neomycin, 3.6 mM for unlabeled TAR with ribostamycin, and 1.3 mM for $^{13}C/^{15}N$-labeled TAR with neomycin. For both aminoglycosides, 1:1 and 2:1 (antibiotic/RNA) unlabeled samples were prepared. Resonance assignment and NOE intensities for the RNA and aminoglycoside components of the complex were obtained from the following experiments: 1) two-dimensional NOESY, two-dimensional TOCSY, and two-dimensional DQF-COSY with unlabeled samples; 2) two-dimensional ^1H-^{13}C ct-HSQC, two-dimensional ^{13}C-filtered NOESY, two-dimensional ^{13}C-filtered TOCSY, three-dimensional HCCH-COSY, three-dimensional HCCH-TOCSY, and three-dimensional ^{13}C-edited NOESY-HSQC with a sample containing uniformly $^{13}C/^{15}N$-labeled adenosines, cytidines, and uridines and unlabeled guanosines. The two-dimensional NOESY spectra were collected with 80-, 150-, 200-, and 400-ms mixing time; the three-dimensional NOESY spectra were collected with 150- and 200-ms mixing time. The DIPSI2rc sequence (18) was used for spin lock in the TOCSY experiments. In the ^{13}C-filtered experiments, ^{13}C magnetization was removed by two subsequent INEPT transfers prior to the two-dimensional NOESY (or TOCSY) pulse sequence. Thus, only cross-peaks between ^{12}C-bound protons were observed in the two spectra. In the NOESY spectrum also, NOEs between ^{12}C-bound and ^{13}C-bound protons were detected. Water suppression was achieved by excitation sculpting (19) or, in experiments with D_2O samples, by presaturation. Shigemi microtubes were used throughout.

All NMR data were processed and analyzed with the program packages NDee and Xndee (SpinUp Inc., Dortmund, Germany), XWIN-NMR (Bruker, Karlsruhe, Germany), and in-house software. Chemical shift values δ from the titration experiments were fitted to the equation,

$$\delta = \frac{1}{2[\mathrm{R}]}\{([\mathrm{A}] + n[\mathrm{R}] + K_D) - \sqrt{([\mathrm{A}] + n[\mathrm{R}] + K_D)^2 - 4n[\mathrm{R}][\mathrm{A}]}\}(\delta_b - \delta_f) + \delta_f \quad \text{(Eq. 1)}$$

where K_D is the dissociation constant, [R] is the concentration of RNA, [A] is the concentration of the antibiotic, n is a factor describing the binding stoichiometry, and δ_f and δ_b are the chemical shift values of free and bound protons of TAR, respectively (20).

Experimental Restraints for Structure Calculation—Intramolecular interproton distance restraints were obtained from two- and three-dimensional NOESY spectra recorded with mixing times of 80, 150, and 200 ms. All NOEs were classified according to their intensity in the spectra as strong (0–3.5 Å), medium (0–4.5 Å), weak (0–5.5 Å), or very weak (0–6.5 Å). NOEs that were observed only in the 400-ms NOESY spectrum were assumed to be extremely weak (0–7.5 Å). Canonical distance restraints were employed to define the hydrogen-bonding pattern and the planarity of the base pairs (21, 22) when strong cross-peaks were observed between the cytidine amino protons and the guanosine H-1 and between the adenosine H-2 and the uridine H-3.

Structure Calculations—Structure calculations were performed using the X-PLOR package, version 3.851 (23). As starting structure for the calculation of the neomycin-bound TAR, a hybrid structure consisting of the stem from the crystal structure of TAR in the presence of Ca^{2+} (24) (Nucleic Acid Data Bank accession code URX075) and the loop (C^{30} through A^{35}) of the solution structure of free TAR (25) (Protein Data Bank (New Brunswick, NJ) accession code 1ANR) was used. The hybrid was constructed by combining coordinates from both structures and performing an energy minimization with X-PLOR. This structure served as template for subsequent structure calculations. The geometry of neomycin was adopted from the structure of a paromomycin-16 S rRNA complex by replacing the ring I C-1′ OH-group of paromomycin by an NH_2-group. The structure calculation comprised three stages. 1) Calculation of the structure of the neomycin-bound TAR was performed, omitting neomycin. This procedure was intended to establish the correct overall RNA fold on the basis of the intramolecular RNA NOEs observed for the neomycin-bound form. For this part of the calculation, the protocol "refine_gentle.inp" supplied with the X-PLOR program package was used (23). 20 ps of molecular dynamics were simulated at 300 K with 1-fs time steps. 100 RNA structures were obtained by averaging over the dynamic trajectory during the final 10 ps followed by a 1000-step conjugate gradient energy minimization in each calculation. This "gentle" procedure allows for conformational changes of the RNA without sacrificing the RNA-typical geometry. 2) Determination of the location of neomycin in the complex was performed by using 15 intermolecular NOE distance restraints between TAR and neomycin derived from the TAR-ribostamycin and TAR-neomycin complexes in addition to the intramolecular RNA NOEs. For the calculation of the complex structure, the 100 neomycin-bound structures (step 1) served as starting structures. During the simulated annealing, the RNA structure was kept fixed except for A^{22} through G^{26} to allow compensation for wrong spatial arrangements in the neomycin bound structure of the TAR caused by the absence of the antibiotic in step 1. This guaranteed extensive sampling of the conformational space for the aminoglycoside and the bulge in a simulated annealing procedure based on the "global fold" protocol (26). In the first 15 ps of the MD simulation at 1000 K, only NOEs and the hydrogen bonds were used as experimental restraints represented by a soft square well potential function. Then 14 cycles of MD calculation, 1 ps each, were done at 1000 K while the force constant for repulsive van der Waals interactions and the asymptote slope for the NOE potential were gradually increased. Finally, the system was cooled from 1000 to 300 K (29 cycles of MD, 0.5 ps each), followed by a 1000-step energy minimization. 3) Refinement of the 100 complex structures thus obtained was performed using a protocol identical to that in step 1 except for a reduction of the integration time step from 1 to 0.5 fs. The distance restraints used were identical to those in step 2, but the RNA conformation was no longer fixed to obtain the overall correct conformation.

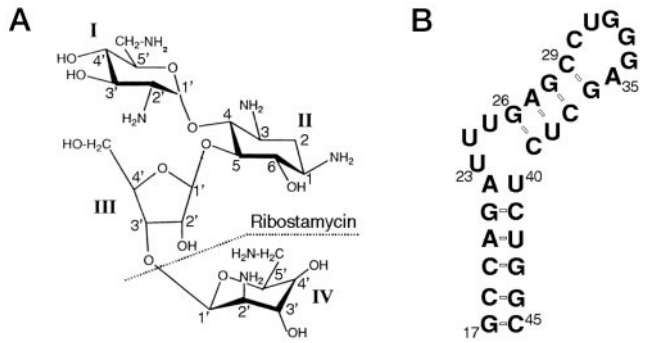

FIG. 1. *a*, the aminoglycosides neomycin and ribostamycin are identical in the first three rings, and neomycin comprises an additional fourth ring. *b*, sequence and secondary structure of the 29-nucleotide TAR; *open boxes* indicate Watson-Crick base pairs.

Out of a total of 100 calculated structures, 17 converged structures with no NOE violation greater than 0.5 Å and no torsion angle violation greater than 3° were accepted and retained for further analysis. Geometry of the structures, structural parameters, and elements of regular secondary structure were determined using the program What_Check (27). SYBYL 6.5 (Tripos Associates) and INSIGHT II (Molecular Simulations, Inc.) were used for visualization of the structures. The coordinates are deposited in the Protein Data Bank (code 1qd3).

RESULTS AND DISCUSSION

Binding of both neomycin B and ribostamycin (see Fig. 1*a*) to HIV-1 TAR was monitored by one-dimensional NMR spectroscopy. Upon the gradual addition of either aminoglycoside to

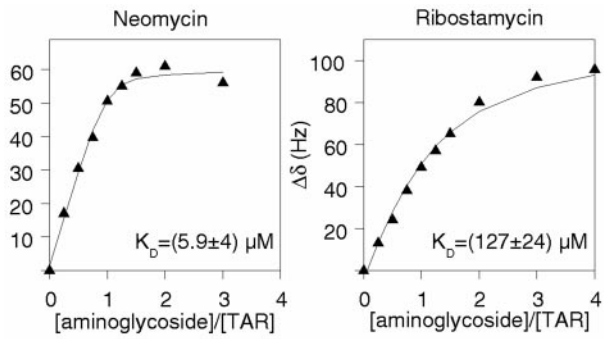

FIG. 2. **Titration of TAR RNA with neomycin (*left*) and ribostamycin (*right*).** To a sample containing 200 μM TAR RNA in 90 mM NaCl, 18 mM potassium phosphate, pH 6.4, H_2O/D_2O (9/1, v/v), each antibiotic was added from a 5.0 mM stock solution in the same buffer. Experiments were performed at 28 °C at 600 MHz. Shown is the change of chemical shift value ($\Delta\delta$) of G^{21} H-1 *versus* the antibiotic/TAR ratio. Dissociation constants (K_D) are calculated by fitting the data to a one-binding site model. For TAR with ribostamycin two additional values with 5 and 10 equivalents of the antibiotic were also used for the fit.

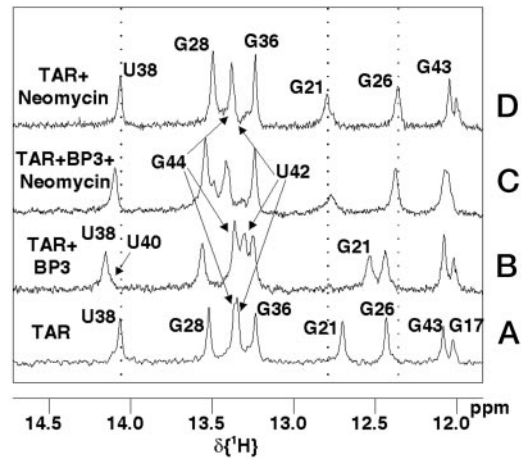

FIG. 3. **One-dimensional imino proton spectra of TAR RNA recorded at 28 °C at 600 MHz.** Sample conditions were 90 mM NaCl, 18 mM potassium phosphate, pH 6.4, H_2O/D_2O (9:1, v/v). To a 200 μM TAR sample (*a*) one equivalent of the Tat peptide BP3 (*b*) or neomycin (*d*) was added from a 5.0 mM stock solution. The sample containing BP3 and neomycin (*c*) was produced by adding one equivalent of neomycin to the TAR-BP3 sample. For free TAR, all peaks are labeled, in the presence of Tat, and neomycin G^{44} and U^{42} were not assigned. *Dotted lines* indicate that resonances in the presence of both Tat and neomycin are closer to the frequencies observed in the presence of neomycin alone than in the presence of Tat alone.

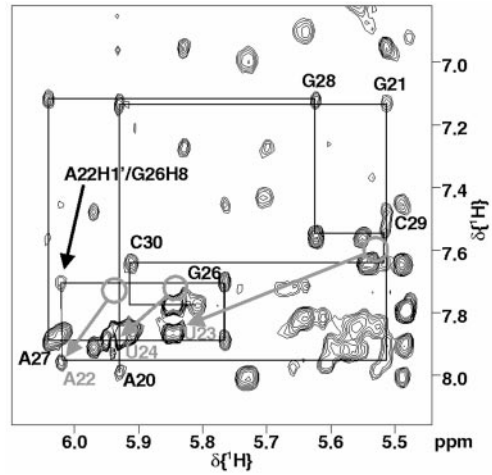

FIG. 4. **Two-dimensional NOESY spectrum of TAR in the presence of neomycin.** The spectrum was recorded at 28 °C at 600 MHz with a mixing time of 150 ms. The sample contained 2.0 mM TAR and 4.0 mM neomycin in 90 mM NaCl, 18 mM potassium phosphate, pH 6.4, H_2O/D_2O (9:1, v/v). H-1′–H-6/H-8 chain tracing is shown from A^{20} through U^{31}, skipping U^{23}–U^{25}. Between A^{22} and G^{26} an NOE is observed (*black arrow*), indicating proximity. *Gray circles* with *arrows* indicate the positions of cross-peaks in the spectrum of free TAR for which the largest shifts are observed upon the addition of neomycin; for U^{23} and U^{24}, the H-5/H-6 cross-resonance is shown.

TAR the resonances of the imino protons in one-dimensional NMR spectra broadened, and several resonances showed continuous changes of their chemical shifts indicating binding. This was also confirmed from UV melting curves of TAR, which show significant changes in the presence of either antibiotic. The NMR imino proton spectrum of TAR in the presence of either aminoglycoside showed one set of resonances, demonstrating that free and aminoglycoside-bound TAR exchange in the intermediate to fast region of the NMR time scale.

Resonances indicating hydrogen bonding and formation of Watson-Crick base pairs are observed for all base pairs in the stem, except for A^{22}-U^{40}, which is located directly below the triple-U bulge. The most pronounced shifts of imino proton resonances are observed for G^{21}, U^{42}, and G^{26}. The imino proton of G^{21} shows a resolved signal over the whole titration range. The neomycin-containing sample aggregated if more than three equivalents of the antibiotic were added to TAR. For ribostamycin, no aggregation was observed for ratios up to 10 equivalents of the aminoglycoside. An equation describing complex formation was fitted to the changes of the chemical shift of G^{21} H-1 (Fig. 2) as described under "Materials and Methods." The only satisfactory fit was achieved with the assumption of a 1:1 complex formation with either aminoglycoside, and the binding constant was calculated to be 5.9 ± 4 μM for neomycin and 127 ± 24 μM for ribostamycin. Due to the lack of values for higher excesses of neomycin, the uncertainty of the latter K_D value was higher. This K_D is of the same order as the K_D of 0.92 μM for neomycin complexed with the TAR 24U→C variant by gel retardation experiments (16).

Neomycin Inhibits Tat Binding to TAR—The Tat-derived peptides BP1 and $BP1_{SW}$ have been shown to have very similar properties with respect to TAR binding as full-length Tat (29, 30). The $BP1_{SW}$-derived peptide BP3 with the amino acid sequence YHSQVWFITKGLGISYGRKKRGQSLTPSQGGQT-HQDPIPKQ has been selected by phage display as a high affinity TAR-binding peptide (31). TAR in the presence of BP3 shows an imino proton spectrum (Fig. 3*b*) characteristic for a conformation that is also observed in the presence of $BP1_{SW}$ or other Tat-derived peptides (28, 32) and thus may indicate the Tat-bound conformation. After the addition of one equivalent of neomycin to the 1:1 TAR/BP3 sample, the spectrum of the imino protons of TAR changed (Fig. 3*c*) and strongly resembled the spectrum of TAR in the presence of neomycin alone (Fig. 3*d*), suggesting that neomycin changes the Tat-bound conformation of TAR. Compared with the corresponding spectrum in the presence of Tat peptides, a completely different resonance pattern is observed. The imino proton resonances of G^{26} and U^{38} are shifted toward the frequency of neomycin bound TAR. Both bases are directly involved in Tat binding (33). The G^{21} imino proton shows a large upfield shift in the Tat-bound conformation. After the addition of neomycin, the resonance is downfield shifted as in the presence of neomycin alone. This clearly confirms competition experiments by gel retardation and CD spectroscopy (12, 16), indicating that the aminoglycoside is able to cause dissociation of Tat peptides from TAR. The results obtained at nano- and micromolar concentrations are thus also valid at millimolar concentrations, and, consequently, NMR spectroscopy is a suitable method to examine TAR-neomycin interaction.

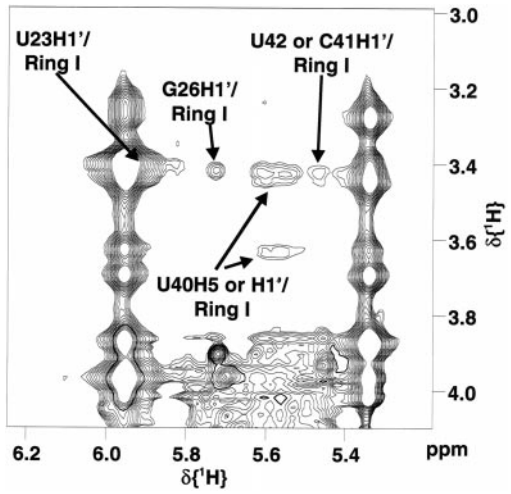

FIG. 5. **Two-dimensional NOESY spectrum of TAR in the presence of ribostamycin.** The spectrum was recorded at 35 °C at 600 MHz with a mixing time of 200 ms. The sample contained 3.6 mM TAR and 7.2 mM ribostamycin in 90 mM NaCl, 18 mM potassium phosphate, pH 6.4, D_2O. The two vertical peak ladders are intramolecular ribostamycin NOEs from H-1′ of rings I and III. Intermolecular NOEs are indicated. Resonances at 3.42 ppm originate either from ring I H-2′ or ring I H-4′; the resonance at 3.63 ppm originates from ring I H-6′ or H-6″. In the presence of neomycin, these NOEs are also observed, but it cannot be distinguished whether they originate from ring I or ring IV due to frequency degeneration. The U^{23} H-1′-ring I (H-2′ or H-4′) cross-peak that is only observed as a shoulder of an intramolecular peak is resolved in the presence of neomycin. The G^{26} H-1′–ring I H-2′/H-4′ NOE together with the C^{41}/U^{42} H-1′–ring I H-2′/H-4′ NOE places ring I in the minor groove, since both NOEs cannot be satisfied if ring I is positioned in the major groove.

BP3-TAR-neomycin samples with an excess of neomycin could not be prepared because of irreversible aggregation that occurred as soon as more than one equivalent of neomycin was added to the BP3-TAR sample. Thus, no further information on the kinetics of the competition could be deduced from our experiments.

Structure Determination—To further characterize the TAR-neomycin complex, we determined the neomycin-bound structure of TAR RNA in solution. For resonance assignment in two- and three-dimensional NMR spectra, we used unlabeled samples containing TAR and one or two equivalents of neomycin or ribostamycin and a 1:1 TAR-neomycin sample in which all adenosines, cytidines, and uridines were completely $^{15}N/^{13}C$-labeled. In addition to standard homonuclear two-dimensional (NOESY, DQF-COSY, and TOCSY) and heteronuclear three-dimensional NMR experiments (^{13}C HSQC-NOESY, HCCH-COSY, and HCCH-TOCSY), ^{13}C-half-filtered experiments (NOESY and TOCSY) proved necessary for the assignment of the RNA resonances. In these experiments, the ^{13}C magnetization is removed prior to the NOESY or TOCSY transfer, and thus only resonances from guanosine protons were observed in the partially labeled sample, rendering H-1′–H-8 resonance assignments of all guanosine protons possible. Sequential NOEs between protons from guanosines and protons from labeled nucleotides could be distinguished from cross-resonances overlapping in standard homonuclear spectra. Despite the strong degeneration of the ribose H-3′, H-4′, H-5′, and H-5″ resonances, 61% of the ribose resonances could be assigned unambiguously.

The strongest shifts (>0.2 ppm) upon aminoglycoside binding were observed for the H-5–H-6 cross-resonances of U^{23} and U^{24} and for the H-1′–H-8 cross resonance of A^{22} in the presence of either antibiotic (Fig. 4). Mapping all shifts larger than 0.05 ppm renders the binding region for the antibiotics well localized; it spans from the bulge, including G^{26}, to the lower stem down to base pair C^{19}-G^{43}. No resonance shifts are observed in the upper stem, except for G^{26}, which is directly flanking the binding region, and for G^{28} H-8. This shift can be attributed to changes in the location of U^{25} caused by a new bulge conformation.

Structural reorganizations indicated by chemical shift mapping are reflected in new NOEs that are observed in the presence of either neomycin or ribostamycin, whereas the NOE pattern in the loop and upper stem remains unchanged. This indicates that no structural changes take place in this part of TAR and that G^{28} is not directly involved in antibiotic binding. Several NOEs are observed between A^{22} and G^{26} (Fig. 4), indicating base stacking of these two nucleotides, and between U^{23} and G^{26}. In the presence of either aminoglycoside, a sequential H-1′–H-8/H-6 walk is possible from G^{17} through U^{31}, except for U^{23} through U^{25} (Fig. 4).

TABLE I
15 intermolecular distance restraints derived from TAR-neomycin and TAR-ribostamycin spectra

Most protons of ring I and ring IV are frequency-degenerated. If NOEs were observed with both neomycin and ribostamycin, NOEs were assigned to ring I protons. For G^{44} H-8, neither NOE was observed with ribostamycin; thus, it was assigned to ring IV protons.

TAR proton	Neomycin proton	Distance interval
		Å
G^{26} H-1′	Ring I H2′ or H4′	4.0
G^{26} H-1′	Ring I H6′ or H6″	5.0
G^{26} H-1′	Ring I H3′	5.5
U^{40} H-1′ or H-5	Ring I H2′ or H4′	5.5
U^{40} H-1′ or H-5	Ring I H3′	6.5
U^{40} H-1′ or H-5	Ring I H6′ or H6″	6.0
C^{41} or U^{42} H-1′	Ring I H4′ or H2′	5.0
G^{21} H-1′	Ring II H3	6.5
G^{21} H-8	Ring III H1′	7.5
G^{21} H-8	Ring III H3′	7.5
U^{23} H-5	Ring I H2′	5.5
U^{23} H-1′	Ring I H2′	4.5
G^{43} H-1′	Ring II H6	6.5
G^{44} H-8	Ring IV H3′	6.5
G^{44} H-8	Ring IV H6′ or H6″	6.5

TABLE II
Structural statistics

Parameter	Value
Average energy (kcal/mol)[a]	
E_{total}	−228.43 (±55.10)
E_{bond}	24.52 (±3.05)
E_{angle}	190.09 (±11.88)
$E_{improper}$	76.16 (±2.82)
E_{vdW}	−346.21 (±27.00)
E_{elec}	−191.40 (±60.80)
E_{NOE}	89.43 (±16.79)
E_{cdih}	1.03 (±0.44)
r.m.s. deviation from ideal distances (Å)	
NOE	0.061
Bond length	0.004
r.m.s. deviation from ideal angles (degrees)	
Bond angles	0.92
Improper angles	0.92
Dihedral angles	0.10
Heavy atom r.m.s. deviation for 17 lowest energy complex structures (Å)	
RNA[b]	2.28
Neomycin	1.32
RNA-neomycin complex[b]	2.25

[a] E_{NOE} and E_{cdih}, NOE energy and dihedral angle energy resulting from a square well potential function with force constants of k_{NOE} = 50 kcal·mol^{-1}·Å^{-2} and k_{cdih} = 10 kcal·mol^{-1}·Å^{-2}.

[b] r.m.s. deviation was calculated for the RNA except the loop region (C29–G36).

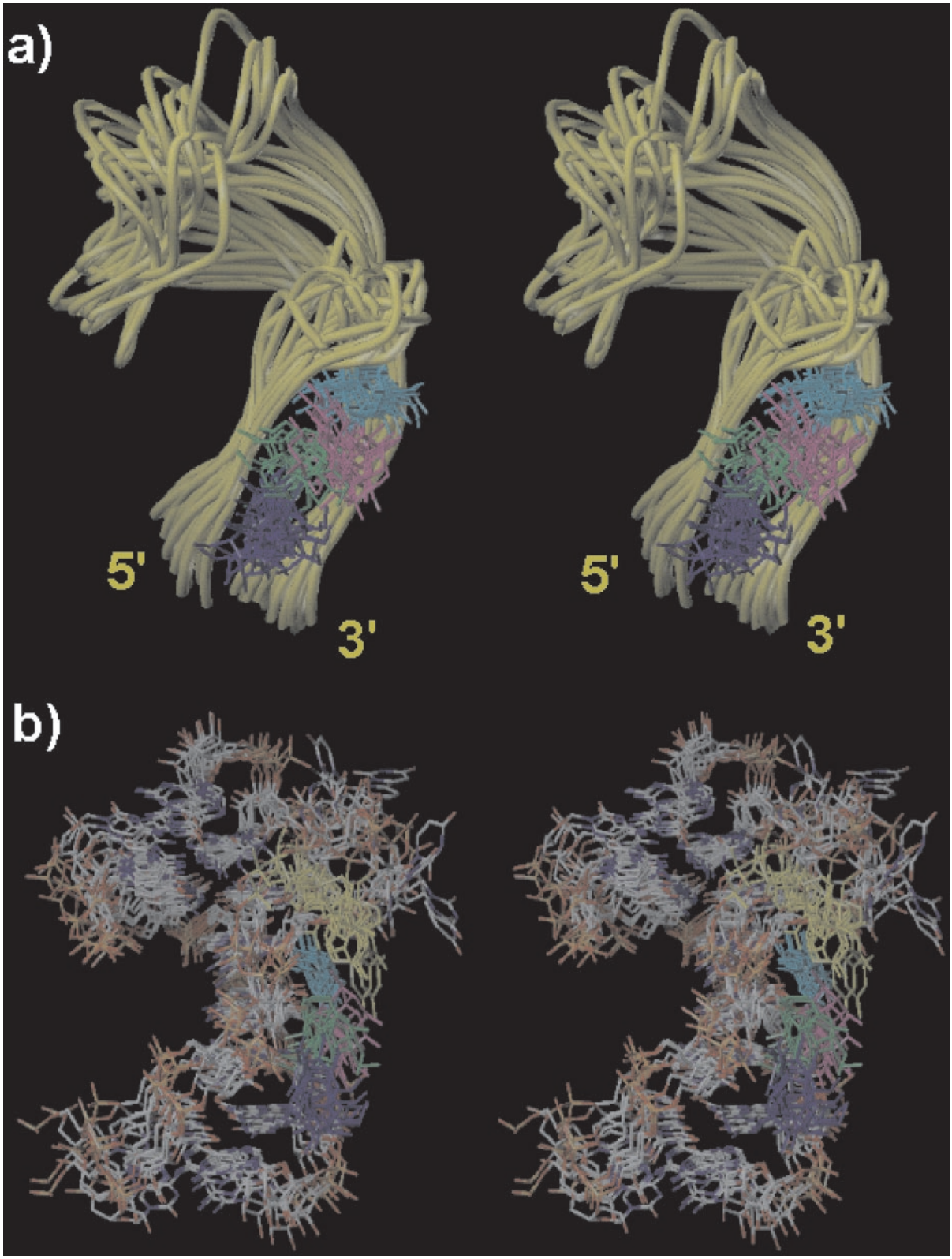

FIG. 6. *a*, stereoview of the 17 lowest energy structures of the TAR-neomycin complex. TAR RNA is represented by a *yellow tube* following the phosphate backbone. Neomycin is represented by *sticks*, and rings have different *colors*, *cyan* (I), *magenta* (II), *green* (III), and *blue* (IV). The drug is bound in the minor groove in the lower stem and bulge region of TAR. The stem is well defined, and the apical loop and the bulge show more flexibility. *b*, stereoview of the eight lowest energy structures of the TAR-neomycin complex. Hydrogen atoms are not shown. Of TAR RNA, only nucleotides 18–28 and 37–44 are shown. Orientation and color coding of neomycin are as in *a*; U^{23} is *yellow*.

Several intermolecular NOEs between neomycin and TAR can be observed in the two-dimensional spectra, but line broadening and low intensity of these signals, which can be attributed to the dynamic properties of the neomycin-TAR complex, do not allow complete assignment of resonances to individual protons. Only two very weak cross-peaks were identified as originating from G^{44} H-8. In the three-dimensional spectra, all intermolecular NOEs were below the limit of detection. In the

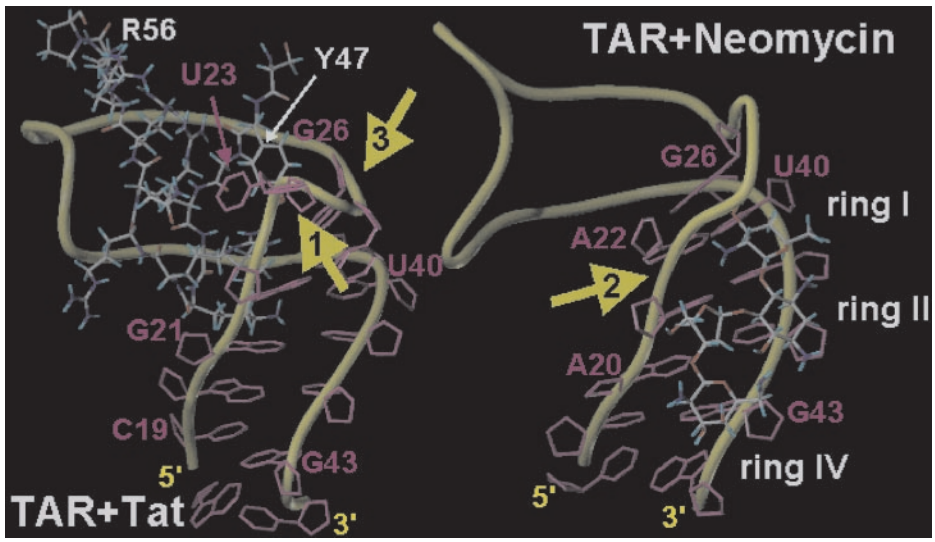

FIG. 7. **Comparison of the Tat-TAR complex model (*left*) (36) with the neomycin-TAR complex (*right*).** The *yellow tube* follows the phosphate backbone of the RNA. Bases and riboses of the neomycin binding region of TAR, Tat-(46–58), and neomycin are shown as *sticks*. The *arrows* indicate structural differences as follows. *Arrow 1*, in the presence of Tat, the phosphate backbone at U^{23} protrudes toward the major groove. In the presence of neomycin, this part of the backbone is bent toward the minor groove, forming a binding pocket for the antibiotic. *Arrow 2*, in the presence of neomycin, the backbone below the bulge is bent toward the major groove. This causes dislocation of the bases G^{21} and A^{22} and a reduction of the volume of the Tat-binding pocket in the major groove. *Arrow 3*, in the presence of Tat, the upper bulge at U^{25} is bent toward the minor groove, leaving a cavity into which Tyr^{47} may bind. In the presence of neomycin, the upper bulge is displaced toward the major groove occupying the binding cavity for Tyr^{47}.

presence of ribostamycin, both RNA and aminoglycoside resonances are significantly less broadened, and spectral overlap is less severe than with neomycin, rendering assignment of all aminoglycoside resonances possible (Fig. 5). Several intermolecular NOEs between TAR and ribostamycin were unambiguously assigned to protons of the antibiotic. RNA frequency degeneration in the two-dimensional spectra, however, still left ambiguities.

The lack of a sufficient number of unambiguous distance restraints led us to calculate the structure of the neomycin-TAR complex in two steps. First, we determined the neomycin-bound structure of TAR, omitting the aminoglycoside molecule in the calculations. From two- and three-dimensional NMR spectra of TAR in the presence of neomycin, we derived 365 intramolecular NOE distance restraints to calculate a set of 100 structures of neomycin-bound TAR.

Chemical shift mapping and observation of identical intramolecular NOE patterns in the presence of either neomycin or ribostamycin resulted in the conclusion that neomycin and ribostamycin bind to the same region of TAR. Thus, intermolecular NOEs observed for the ribostamycin complex were considered valid also for neomycin. Given the identity of the first three rings in both aminoglycosides, binding according to the same mechanism is to be expected. Neamine, which is identical to neomycin and ribostamycin in the first two rings, causes changes in the chemical shifts of protons from the same region of TAR as observed for ribostamycin and neomycin, and in other neomycin-RNA complexes contacts responsible for binding specificity are established by atoms from the first two neomycin rings (2, 7). In the tobramycin-RNA complex structures, it is also the 2-deoxystreptamine ring (ring II) that is responsible for specific intermolecular contacts (6).

The present chemical shift data and, independently, RNase footprinting data (16) indicate that the aminoglycoside binding region stretches from C^{19} to G^{26} and from U^{40} to G^{43}. Thus, intermolecular NOEs were assumed to originate only from protons of nucleotides that are part of or flanking this proposed binding region, while no assumption on minor or major groove binding was made.

Using this strategy, 13 intermolecular distance restraints could be derived from the NMR spectra (Table I) of the RNA-ribostamycin complex, and two ambiguous NOEs observed in the neomycin complex could be assigned unambiguously on the basis of the ribostamycin data. No single strong intermolecular key NOE that *a priori* allows us to place the aminoglycoside in either the minor or the major groove was identified. NOEs are found between protons of the aminoglycoside and protons of the RNA that are accessible from the minor groove as well as protons accessible from the major groove, a fact that is not surprising, since protons of a ligand bound in the minor groove are expected to be closer than 5 Å to protons in the major groove, and *vice versa*. However, the combination of the uniquely observed NOEs defines the binding site of the antibiotic. The origin of several pairs of NOEs, for example G^{26} H-1′–ring I H-2′/H-4′ and C^{41}/U^{42} H1′–ring I H-2′/H-4′ (Fig. 5), cannot be explained by binding of the antibiotic to the major groove of TAR and thus places the drug in the minor groove. Further support for minor groove binding is given by the chemical shift data. A binding pocket in the major groove would always include nucleotides of the upper stem for which no significant changes of chemical shift values were observed upon complex formation, rendering major groove binding unlikely.

Structure Calculations Place Neomycin in the Minor Groove of TAR—The NOE-derived intermolecular distances were then used as a starting point for structure calculations of the RNA-neomycin complex; to 100 structures of neomycin-bound TAR that resulted from the MD calculations the aminoglycoside was added. Using the RNA-ribostamycin-derived distance restraints, a simulated annealing calculation with subsequent refinement resulted in 17 converged structures with no NOE violations larger than 0.5 Å (Table II).

In none of the calculated models was the aminoglycoside bound in the major groove, reflecting the fact that the set of NOE-derived distance restraints is only compatible with minor groove binding. The structure of neomycin and the stem region of TAR are well defined in the complex. Neomycin is bound in the TAR RNA minor groove, with rings I and II under the triple-U bulge. Ring III is located in the minor groove close to G^{21}, and ring IV spans the minor groove contacting both A^{20}

and G^{43} (Fig. 6). Stacking of A^{22} and G^{26} allows formation of a continuous helix in the RNA stem. A^{22} and U^{40} form a Watson-Crick base pair not obvious from the experimental data and therefore not introduced by hydrogen bonding restraints in the calculations. Both bases are propeller-twisted and buckled against each other, explaining the absence of a strong imino proton signal of U^{40}. The minor groove is widened from C^{19}:G^{43} to A^{22}:U^{40} compared with an ideal A-helix.

The definition of the apical loop and the triple-U bulge is low, reflecting conformational flexibility of these regions (Fig. 6). In all 17 structures, a binding pocket is formed in the deepened minor groove. Bordering on this pocket is the base of G^{26} that is shifted toward the minor groove relative to A^{22}. Rings I and II of neomycin are enclosed by the protruding phosphate backbone of the bulge and by its bases. Thus, the aminoglycoside is buried in the minor groove, and its accessible surface is reduced by more than 50% compared with the free molecule. The TAR-neomycin complex is thus substantially different from other well defined RNA-aminoglycoside complexes in which the antibiotic is bound in the major groove of the RNA.

Although the location of the bases of the bulge is not well defined, the backbone of the bulge shows that the conformation differs significantly from all published TAR conformations; in free TAR, the bulge spans a gap of nearly 10 Å between A^{22} and G^{26} (25); in the proposed Tat-bound conformation, U^{23} is in the major groove, U^{25} is in the minor groove, and C^{24} is exposed, while the phosphate of C^{24} protrudes from the backbone (32); in the presence of Ca^{2+} ions, the bulge adopts yet another conformation, with all three bases stacked above the backbone, which is looped out toward the apical loop, and U^{23} on the minor groove and U^{25} on the major groove side (24). None of the published TAR structures shows a cavity in the minor groove formed by the backbone or bases of the bulge. Neomycin thus induces a conformation of the uridine-rich bulge that differs from all known TAR structures.

How Neomycin Inhibits Tat Binding—In the presence of neomycin, the volume of the major groove into which Tat binds is reduced. This is caused on the one hand by a change of the location of the bulge (Fig. 7) and on the other hand by a shift of the bases of the lower stem toward the major groove. Mutational experiments have shown that U^{23} and G^{26} play a crucial role for Tat binding and cannot be altered without significant loss of binding affinity (34). Regardless of the details of the actual mode of Tat binding, the presence of neomycin is able to disturb intermolecular protein-RNA contacts. The reduced volume of the major groove especially in the lower stem region causes different orientations of U^{23} and G^{26} relative to Tat. The complex thus becomes unstable, and Tat dissociates from the RNA.

In MD simulations in which the neomycin molecule was docked to the free TAR (35), the antibiotic is bound mainly in the major groove, establishing contacts to both the upper and the lower stem and thus stabilizing the conformation of free TAR. In contrast, from our experiments neomycin induces a novel conformation that is rather similar to the Tat-bound one, which, however, does not allow essential contacts between RNA and protein (Fig. 7). Nevertheless, the docking experiments suggested that neomycin contacts O-4 of U^{23} in free TAR. Thus, initial contacts may be formed with U^{23} O-4 before the aminoglycoside is bound to TAR, supporting the notion that a ternary complex is formed from which Tat dissociates after neomycin is bound and TAR has adopted the neomycin-bound conformation (16).

Implications for the Design of Anti-HIV Drugs—A general model for the interaction of cationic antibiotics with RNA suggests that amino groups form specific RNA contacts (14), which may also hold for the TAR-neomycin complex. In all of our calculated final structures, the amino groups of rings I and II are close to possible hydrogen bond acceptors. The amino group of ring I C-2′ is located in the vicinity of G^{21} and A^{22} in all structures; the ring II C-1 amino group is close to the phosphate backbone at U^{42} or O-4 of U^{42}, suggesting that RNA recognition is achieved via the neamine core of the aminoglycosides.

Use of neomycin as an anti-HIV drug would be strongly hampered by its ability to bind to a wide range of RNA structures (1, 8, 9) and to inhibit other biological functions. In all biological systems so far, neomycin is bound deep in the RNA major groove (2, 13, 14), contrasting with the TAR-neomycin complex structure, where part of neomycin ring IV is accessible from the surface (Fig. 6). Thus, additional, bulky groups or even other small molecules attached to ring IV that prevent major groove complexes from being established may be accommodated in this complex, leading to reduction of the toxicity of neomycin while conserving high TAR affinity.

Acknowledgment—We thank Ulrike Herzing for excellent technical assistance.

REFERENCES

1. Moazed, D. & Noller, H. F. (1987) *Nature* **327,** 389–394
2. Fourmy, D., Recht, M. I., Blanchard, S. C. & Puglisi, J. D. (1996) *Science* **274,** 1367–1371
3. Fourmy, D., Yoshizawa, S. & Puglisi, J. D. (1998) *J. Mol. Biol.* **277,** 333–345
4. Yoshizawa, S., Fourmy, D. & Puglisi, J. D. (1998) *EMBO J.* **17,** 6437–6448
5. Jiang, L., Suri, A. K., Fiala, R. & Patel, D. J. (1997) *J. Chem. Biol.* **4,** 35–50
6. Jiang, L. & Patel, D. J. (1998) *Nat. Struct. Biol.* **5,** 769–774
7. Jiang, L., Majumdar, A., Hu, W., Jaishree, T. J., Xu, W. & Patel. D. J. (1999) *Structure* **7,** 817–827
8. von Ahsen, U., Davies, J. & Schroeder, R. (1991) *Nature* **353,** 368–370
9. Stage, T., Hertel, K. J. & Uhlenbeck, O. C. (1995) *RNA* **1,** 95–101
10. Rogers, J., Chang, A. H., von Ahsen, U., Schroeder, R. & Davies, J. (1996) *J. Mol. Biol.* **259,** 916–925
11. Zapp, M., Stern, S. & Green, M. R. (1993) *Cell* **74,** 969–978
12. Mei, H. Y., Galan, A. A., Halim, N. S., Mack, D. P., Moreland, D. W., Sanders, K. B., Truong, H. N. & Czarnik, A. W. (1995) *Bioorg. Med. Chem. Lett.* **5,** 2755–2760
13. Hoch, I., Berens, C., Westhof, E. & Schroeder, R. (1998) *J. Mol. Biol.* **282,** 557–569
14. Hermann, T. & Westhof, E. (1998) *J. Mol. Biol.* **276,** 903–912
15. Leclerc, F. & Cedergren R. (1998) *J. Med. Chem.* **41,** 175–182
16. Wang, S., Huber, P. W., Cui, M., Czarnik, A. W. & Mei, H. Y. (1998) *Biochemistry* **37,** 5549–5557
17. Wei, P., Garber, M. E., Fang, S. M., Fischer, W. & Jones, K. A. (1998) *Cell* **92,** 451–462
18. Cavanagh, J. & Rance, M. (1992) *J. Magn. Res.* **96,** 670–678
19. Hwang, T. L. & Shaka, A. J. (1995) *J. Magn. Res.* **112A,** 275–279
20. Rösch, P., Klaus, W., Auer, M. & Goody, R. S. (1989) *Biochemistry* **28,** 4318–4325
21. Saenger, W. (1984) *Principles of Nucleic Acid Structure*, Springer-Verlag New York Inc., New York
22. Cate, J. H., Gooding, A. R., Podell, E., Zhou, K, Golden, B. L., Kundrot,. E., Cech, T. R. & Doudna, J. A. (1996) *Science* **273,** 1678–1685
23. Brünger, A. T. (1996) *X-PLOR Version 3.851 Online*, Howard Medical School and Yale University, New Haven, CT
24. Ippolito, J. A. & Steitz, T. A. (1998) *Proc. Natl. Acad. Sci. U. S. A.* **95,** 9819–9824
25. Aboul-ela, F., Karn, J. & Varani, G. (1996) *Nucleic Acids Res.* **24,** 3974–3981
26. Varani, G., Aboul-ela, F. & Allain, F. H. T. (1996) *Progr. NMR Spectr.* **29,** 51–127
27. Hooft, R. W. W., Vriend, G., Sander, C. & Abola, E. E. (1996) *Nature* **381,** 272–272
28. Long, K. S. & Crothers, D. M. (1999) *Biochemistry* **38,** 10059–10069
29. Metzger, A. U., Schindler, T., Willbold, D., Kraft, M., Steegborn, C., Volkmann, A., Frank, R. & Rösch, P. (1996) *FEBS Lett.* **384,** 255–259
30. Metzger, A. U., Bayer, P., Willbold, D., Hoffmann, S., Frank, R., Goody, R. S. & Rösch, P. (1997) *Biochem. Biophys. Res. Commun.* **241,** 31–36
31. Hoffmann, S. (1998) *In vitro- und in vivo-Selektion an den lentiviralen Transaktivator Proteinen aus HIV- 1 und EIAV*, Ph.D. thesis, University of Bayreuth
32. Aboul-ela, F., Karn, J. & Varani, G. (1995) *J. Mol. Biol.* **253,** 313–332
33. Hamy, F., Asseline, U., Grasby, J., Iwai, S., Pritchard, C., Slim, G., Butler, P. J. G., Karn, J. & Gait, M. (1993) *J. Mol. Biol.* **230,** 111–123
34. Churcher, M. J., Lamont, C., Hamy, F., Dingwall, C., Green, S. M., Lowe, A. D., Butler, J. G., Gait, M. J. & Karn J. (1993) *J. Mol. Biol.* **230,** 90–110
35. Hermann, T. & Westhof, E. (1999) *J. Med. Chem.* **42,** 1250–1261
36. Seewald, M. J., Metzger, A. U., Willbold, D., Rösch, P. & Sticht, H. (1998) *J. Biomol. Struct. Dyn.* **16,** 683–692